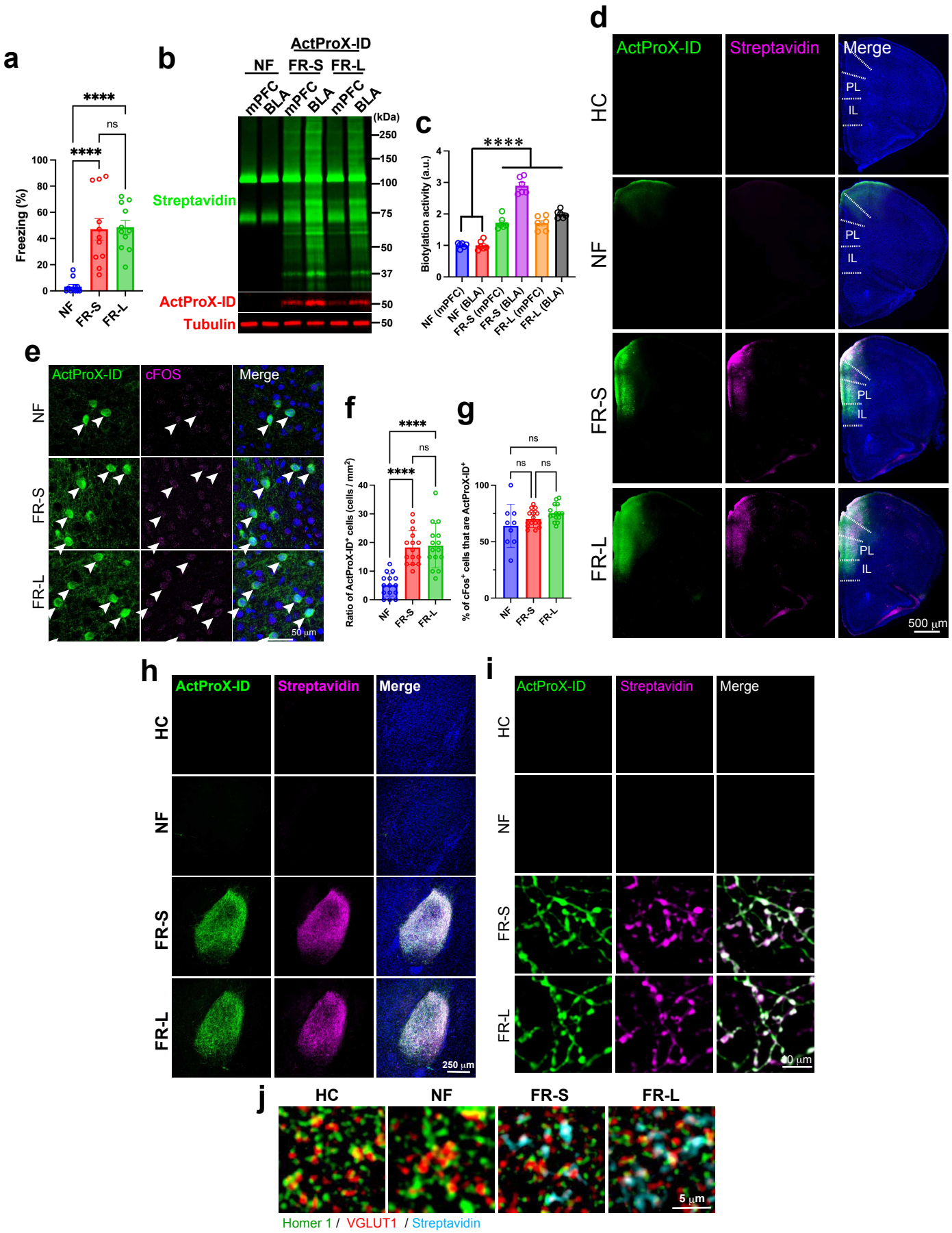

Extended Data Fig. 1. Behavioural state–dependent ActProX-ID labelling in the mPFC–BLA circuit. a, Freezing during the post-tone period of the cued trial in NF, FR-S and FR-L groups. **b,c**, Immunoblot analysis (**b**) and quantification (**c**) of streptavidin-enriched biotinylated proteins in mPFC and BLA lysates from NF, FR-S and FR-L mice expressing ActProX-ID. **d**, Representative confocal images of mPFC sections from HC, NF, FR-S and FR-L mice expressing ActProX-ID, showing ActProX-ID signal and streptavidin staining and their merge. Scale bar, 500 µm. **e**, Coronal mPFC sections (prelimbic (PL) areas) from NF, FR-S and FR-L mice, showing ActProX-ID signal together with cFos immunostaining and merged images. Scale bar, 50 µm. **f**, Quantification of the density of ActProX-ID–positive cells in the mPFC across NF, FR-S and FR-L groups. **g**, Quantification of the density of cFos-positive neurons that are ActProX-ID–positive in PL across NF, FR-S and FR-L groups. **h**, Representative confocal images showing ActProX-ID–mediated biotinylation in the BLA in HC, NF, FR-S and FR-L groups. Sections were stained with streptavidin to visualise biotinylated proteins in mPFC→BLA presynaptic terminals. Scale bar, 250 µm. **i**, Representative confocal images of ActProX-ID signal and streptavidin staining in the BLA of HC, NF, FR-S and FR-L mice. Scale bar, 10 µm. **j**, Colocalisation of Homer1 and VGLUT1 (excitatory synaptic markers) with streptavidin in biotinylated mPFC→BLA synapses, confirming enrichment at excitatory presynaptic terminals. Scale bar, 5 µm. In **a**, data are mean ± s.e.m.; NF = 11, FR-S = 11 and FR-L = 11 mice. In **c**, data are mean ± s.e.m.; NF = 6, FR-S = 6 and FR-L = 6 mice. One-way ANOVA with Tukey's multiple comparisons test; ****P < 0.0001. In **f** and **g**, data are mean ± s.e.m.; NF = 4, FR-S = 4 and FR-L= 4 mice; one-way ANOVA with Tukey's multiple comparisons test; ****P < 0.0001.

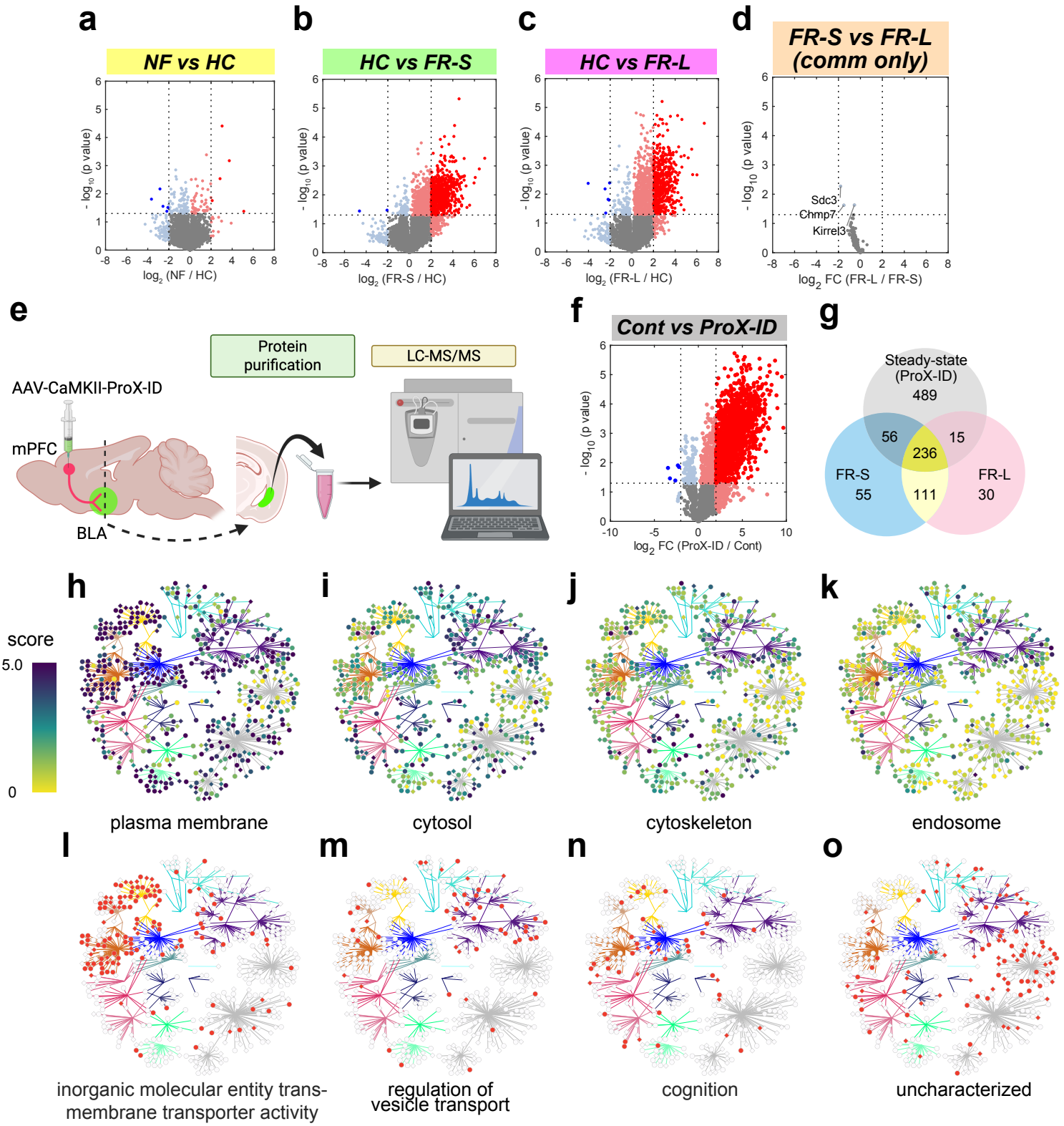

Extended Data Fig 2. Spatiotemporal proteomic landscape of memory recall. **a-c**, Volcano plots showing $\log_2$ (fold change) versus $-\log_{10}$ (P value) for ActProX-ID–labelled proteins in NF(**a**), FR-S (**b**) and FR-L (**c**) samples compared with HC sample. Dotted lines indicate the thresholds used to define recall-responsive proteins. Red dots represent significantly enriched proteins ($\log_2$ fold change > 2.0 and $P < 0.05$). **d**, Volcano plot comparing biotinylation levels of FR-S/FR-L-common proteins between FR-S and FR-L, showing that only a small subset exhibits significantly different abundance across recall phases. **e**, Schematic representation of the ProX-ID approach. **f**, Volcano plots showing $\log_2$(fold change) versus $-\log_{10}$(P value) for ProX-ID–labelled proteins compared with controls. **g**, Venn diagrams summarise the number of proteins enriched in the ProX-ID dataset and their overlap with FR-S-selective, FR-L-selective and FR-S/FR-L-common groups. **h–k**, STRING Compartment Score of Recall-responsive proteins for the selected cellular compartment. **l–o**, Recall-responsive proteins annotated for the selected category are highlighted.

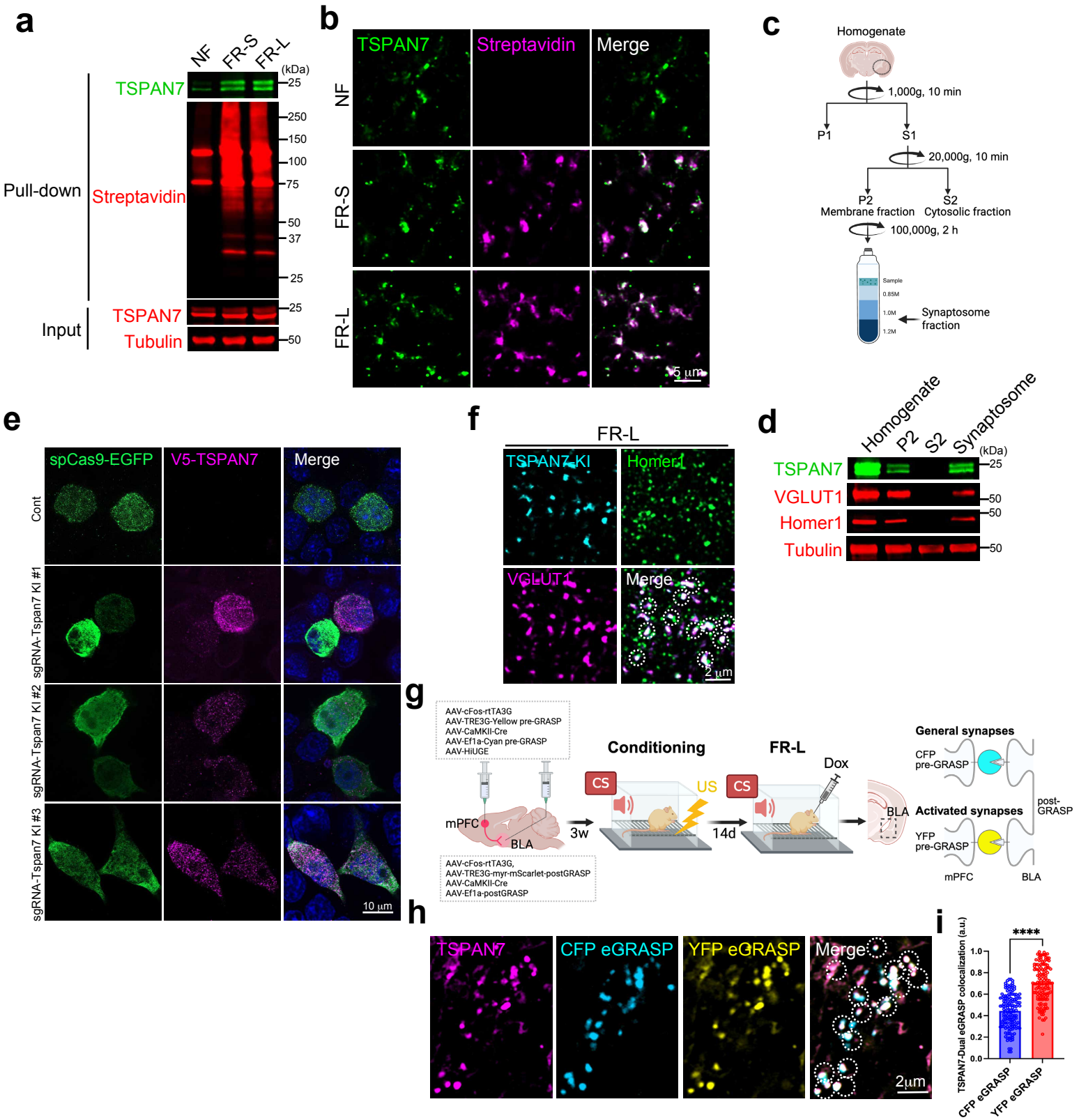

Extended Data Fig. 3. Biochemical validation of TSPAN7 enrichment at ActProX-ID–labelled synapses and of HiUGE-based TSPAN7–V5 knock-in. **a**, Streptavidin pull-down followed by immunoblotting for TSPAN7 in BLA samples from NF, FR-S and FR-L mice expressing ActProX-ID. Input lanes show total TSPAN7 and tubulin. **b**, Representative confocal images of BLA sections from NF, FR-S and FR-L mice stained for endogenous TSPAN7 and streptavidin. Scale bar, 5 μm. **c**, Schematic of the biochemical fractionation protocol used to obtain homogenate, membrane fraction (P2), cytosolic fraction (S2) and synaptosome fraction from BLA tissue. **d**, Immunoblot analysis of TSPAN7, VGLUT1, Homer1 and tubulin across homogenate, P2, S2 and synaptosome fractions. **e**, Representative images of HEK293T cells co-expressing SpCas9–EGFP and HiUGE donor constructs (V5–TSPAN7) together with Tspan7-targeting sgRNAs (sgRNA-Tspan7 KI #1–3). Scale bar, 10 μm. **f**, Confocal images showing colocalisation of TSPAN7–V5 with the excitatory synaptic markers Homer1 and VGLUT1 at mPFC→BLA synapses after FR-L, confirming localisation at glutamatergic presynaptic terminals. Scale bar, 2 μm. **g**, Schematic of doxycycline-gated dual-eGRASP strategy to differentially label total mPFC→BLA synaptic contacts (CFP eGRASP) and behaviourally reactivated synapses (YFP eGRASP) during FR-L. **h**, Representative dual-eGRASP images in the BLA of TSPAN7-V5-KI mice showing TSPAN7 immunostaining relative to cyan (total) and yellow (reactivated) eGRASP puncta. Scale bar, 2 μm. **i**, Quantification of the proportion of CFP- and YFP-eGRASP–labelled synapses that are TSPAN7-positive, showing preferential enrichment of TSPAN7 at behaviourally reactivated (YFP) synapses during FR-L. In **i**, data are mean ± s.e.m.; NF = 15, FR-S = 14 and FR-L = 15 fields from each of 4 mice; Student's t-test; ****P < 0.0001.

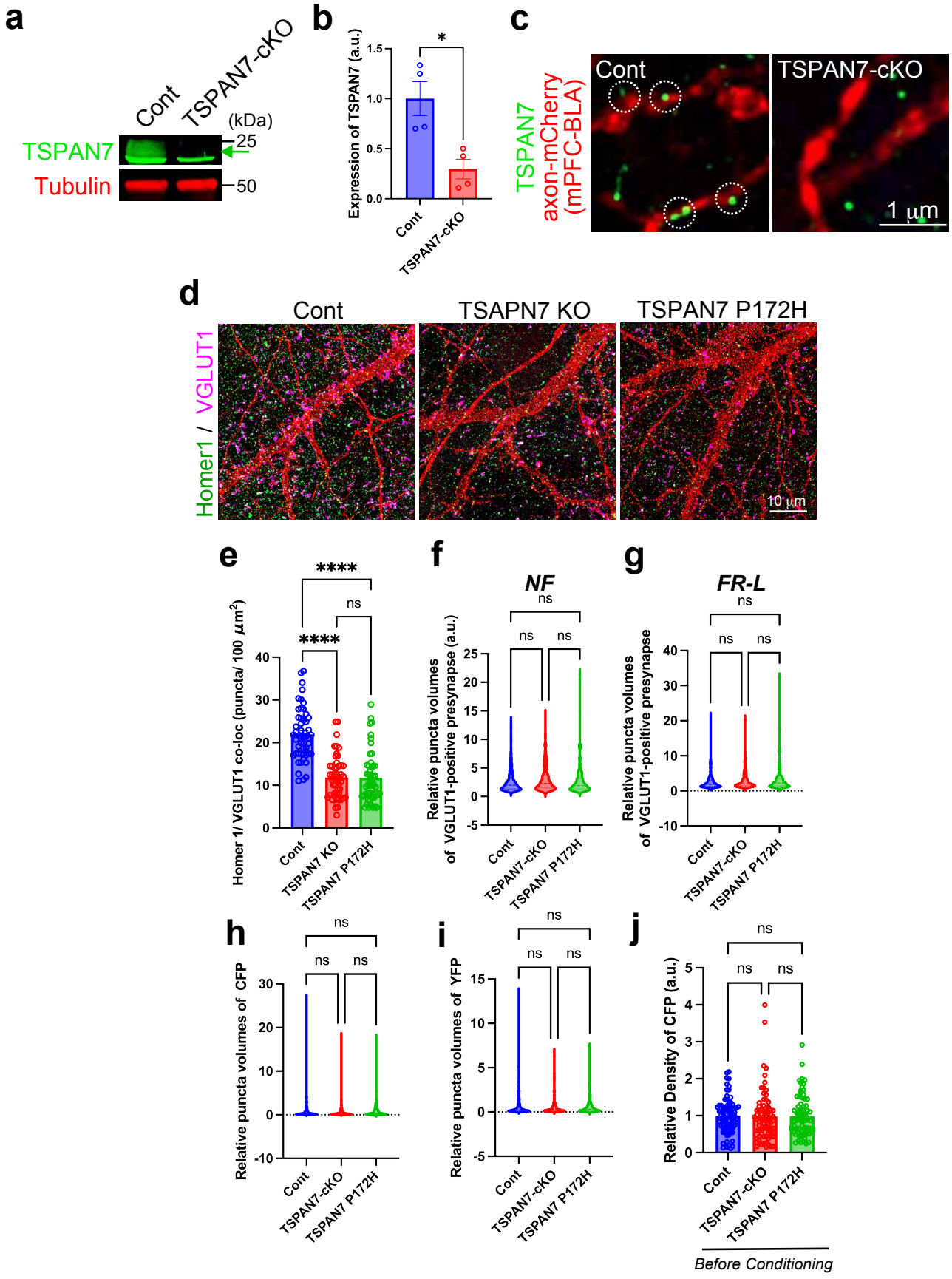

Extended Data Fig. 4. Effects of TSPAN7-cKO and TSPAN7 P172H on synapse formation in the mPFC–BLA pathway. **a**, Immunoblot analysis of TSPAN7 and tubulin in BLA tissue from control and TSPAN7-cKO mice. **b**, Quantification of TSPAN7 expression levels in BLA tissue from control and TSPAN7-cKO mice. **c**, Representative confocal images of BLA sections showing TSPAN7 immunoreactivity at axon-mCherry–labelled mPFC→BLA boutons in control and TSPAN7-cKO mice. Scale bar, 1 μm. **d**, Representative images of Homer1/VGLUT1-positive excitatory synapses in cultured TSPAN7-KO and TSPAN7 P172H neurons. Scale bar, 10 μm. **e**, Quantification of Homer1/VGLUT1-positive excitatory synapse density in cultured TSPAN7-KO and TSPAN7 P172H neurons. **f–g**, Quantification of the volumes of VGLUT1-positive synapses in control, TSPAN7-cKO and TSPAN7 P172H mice across NF (**f**) and FR-L (**g**) conditions. **h–i**, Quantification of the volumes of CFP-positive and YFP-positive synapses in control, TSPAN7-cKO and TSPAN7 P172H mice under FR-L conditions. **j**, Quantification of CFP-positive excitatory synapse density in control, TSPAN7-cKO and TSPAN7 P172H mice before conditioning. In **e**, data are mean ± s.e.m.; Cont = 50, TSPAN7-KO = 50, TSPAN7 P172H = 50 cells from 4 independent experiments; one-way ANOVA with Tukey's multiple comparisons test; ****P < 0.0001. In **f–j**, data are mean ± s.e.m.; Cont = 36, TSPAN7-cKO = 36 and TSPAN7 P172H = 36 from each of 4 mice; one-way ANOVA with Tukey's multiple comparisons test; ns, not significant.

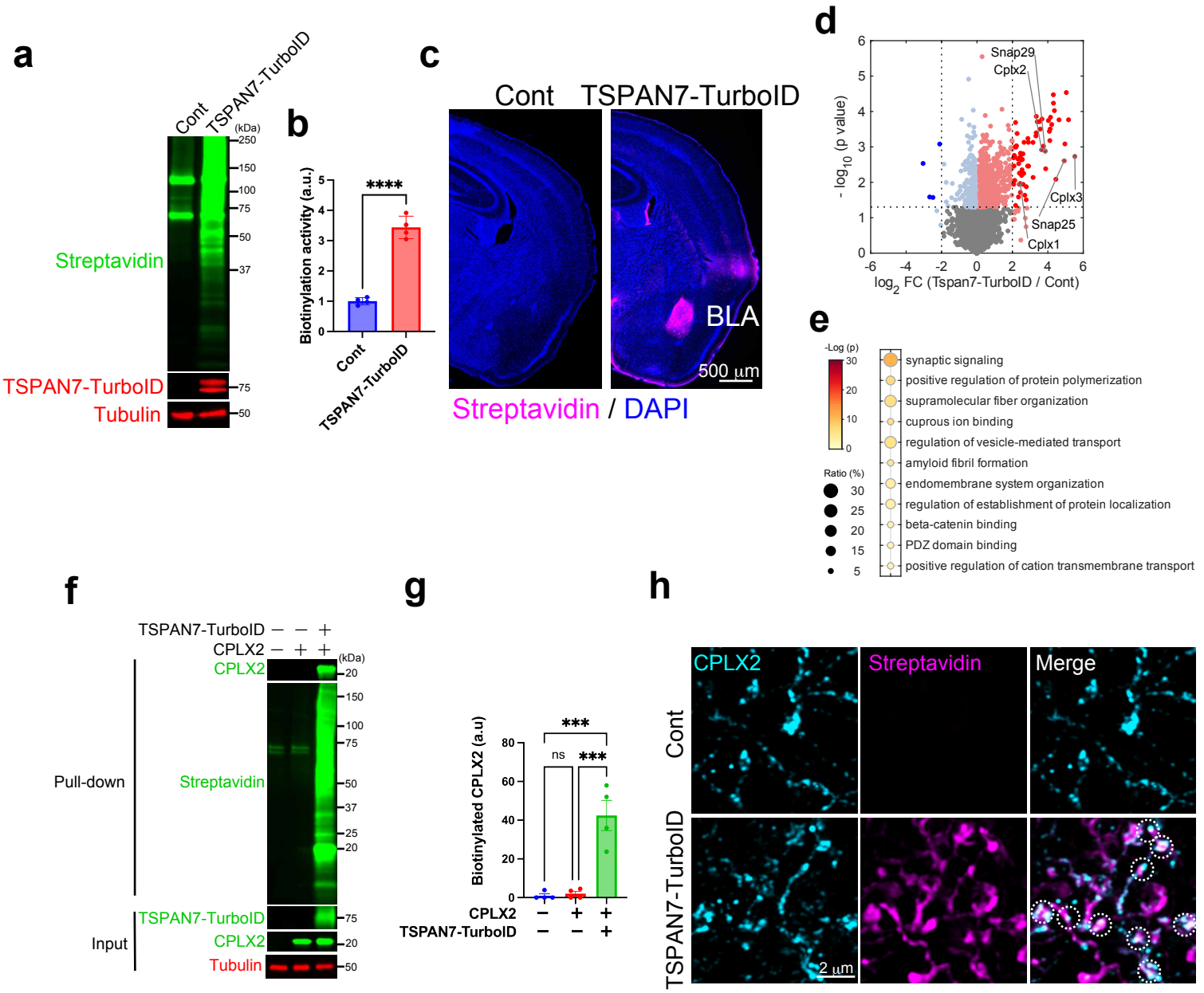

Extended Data Fig. 5. Proteomic characterisation of the TSPAN7–TurboID interactome and validation of CPLX2 as a novel TSPAN7 interactor. **a**, Streptavidin immunoblot of pull-down fractions and input lysates from DIV14 cultured neurons expressing TSPAN7–TurboID. **b**, Quantification of streptavidin signal intensity in cultured neurons expressing TSPAN7–TurboID. **c**, Representative confocal images showing TSPAN7–TurboID–mediated biotinylation in the BLA. Sections were stained with streptavidin to visualise biotinylated proteins in mPFC→BLA presynaptic terminals. Scale bar, 500 µm. **d**, Volcano plot of proteins identified by LC–MS/MS in TSPAN7–TurboID versus control streptavidin pull-down samples. **e**, Gene Ontology enrichment analysis of TSPAN7–TurboID–enriched proteins. **f**, Streptavidin pull-down from the cell lysates of cultured neurons expressing TSPAN7–TurboID with or without co-expressed CPLX2, followed by immunoblotting for CPLX2, streptavidin, TSPAN7–TurboID and tubulin. **g**, Quantification of biotinylated CPLX2 in the presence or absence of TSPAN7–TurboID. **h**, Representative confocal images of BLA sections from control mice and mice expressing TSPAN7–TurboID, stained for CPLX2 and streptavidin. Scale bar, 2 µm. In **b**, data are mean ± s.e.m.; Cont = 4, TSPAN7-TurboID = 4 independent experiments; Student's t-test; ****P < 0.0001. In **g**, data are mean ± s.e.m.; Cont = 4, CPLX2 = 4, CPLX2 + TSPAN7-TurboID = 4 independent experiments; one-way ANOVA with Tukey's multiple comparisons test; ****P < 0.0005.

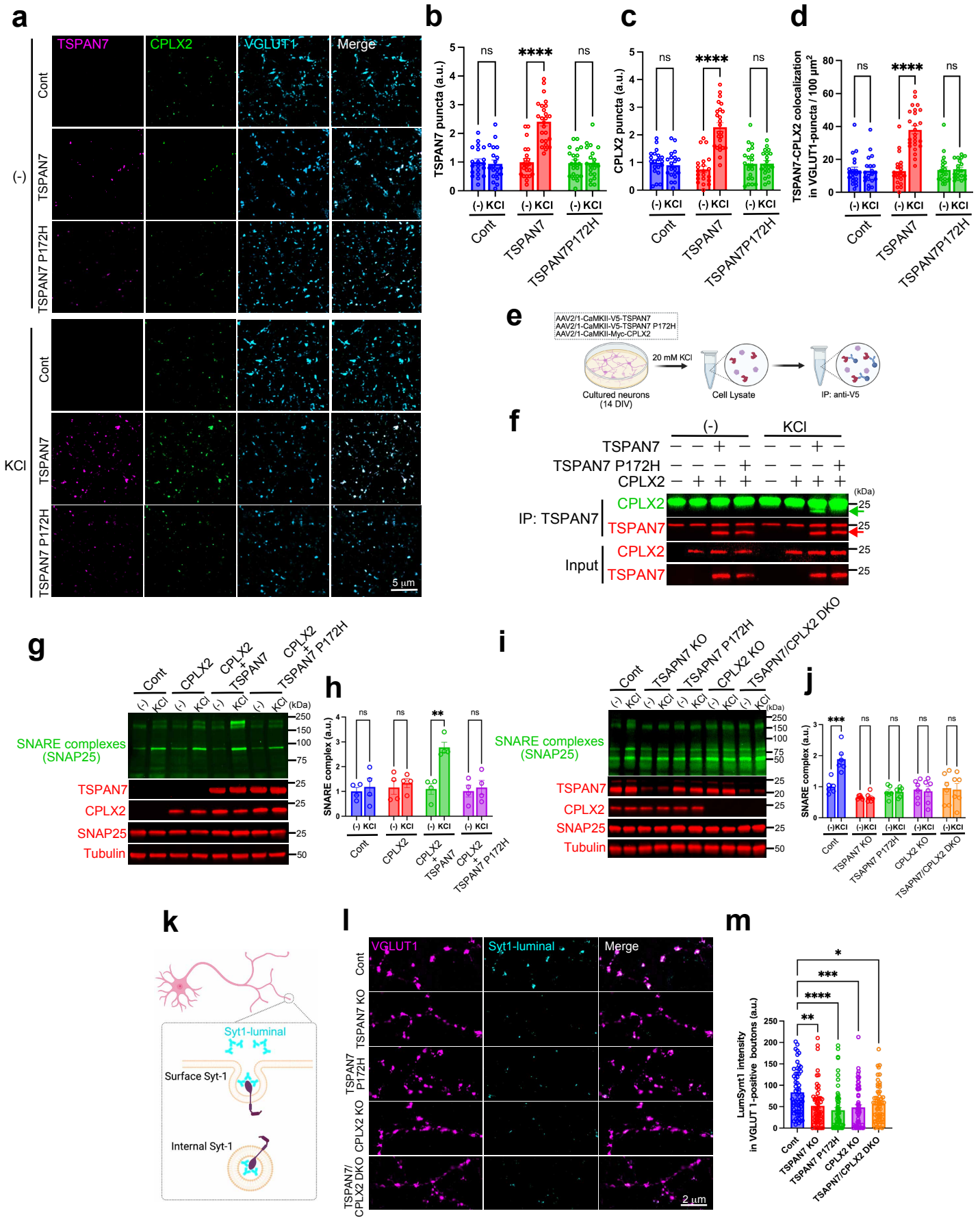

Extended Data Fig. 6. Biochemical and imaging analysis of TSPAN7–CPLX2 complexes and SNARE assembly. a, Representative DIV14 neuron images of TSPAN7, CPLX2 and VGLUT1 in cells expressing TSPAN7 or TSPAN7 P172H under resting conditions or after depolarisation (high KCl). Scale bar, 5 µm. **b–d**, Quantification of TSPAN7, CPLX2 and VGLUT1 intensities and co-localisation at presynaptic sites across genotypes and conditions. **e**, Schematic of co-immunoprecipitation assays testing TSPAN7–CPLX2 interactions at rest and after high KCl. **f**, Representative immunoblots of TSPAN7, CPLX2 and SNAP25 from TSPAN7 immunoprecipitates and inputs. **g–h**, Representative immunoblots and quantification of SNARE complexes (high-molecular-weight SNAP25 bands), TSPAN7 and CPLX2 in DIV14 neurons co-expressing CPLX2 with TSPAN7 or TSPAN7 P172H. **i–j**, Representative immunoblots and quantification of SNARE complexes, TSPAN7 and CPLX2 in TSPAN7-KO, TSPAN7 P172H, CPLX2-KO and TSPAN7/CPLX2-DKO neurons. **k**, Schematic of the Syt1-luminal uptake assay to measure activity-evoked vesicle recycling at VGLUT1-positive boutons after high KCl. **l**, Representative images of VGLUT1 and Syt1-luminal signals. Scale bar, 2 µm. **m**, Quantification of Syt1-luminal intensity at VGLUT1-positive boutons. In **b–d**, mean ± s.e.m.; Cont (–) n=20, Cont (KCl) n=20, TSPAN7 (–) n=21, TSPAN7 (KCl) n=25, P172H (–) n=21, P172H (KCl) n=20 cells (4 independent experiments); one-way ANOVA with Tukey; ****P<0.0001. In **h**, 4 independent experiments; one-way ANOVA with Tukey; **P<0.005. In **j**, n=4 independent experiments per condition; one-way ANOVA with Tukey; **P<0.005. In **m**, n=60 cells per genotype (4 independent experiments); one-way ANOVA with Tukey; ****P<0.0001, ***P<0.001, **P<0.01, *P<0.05.

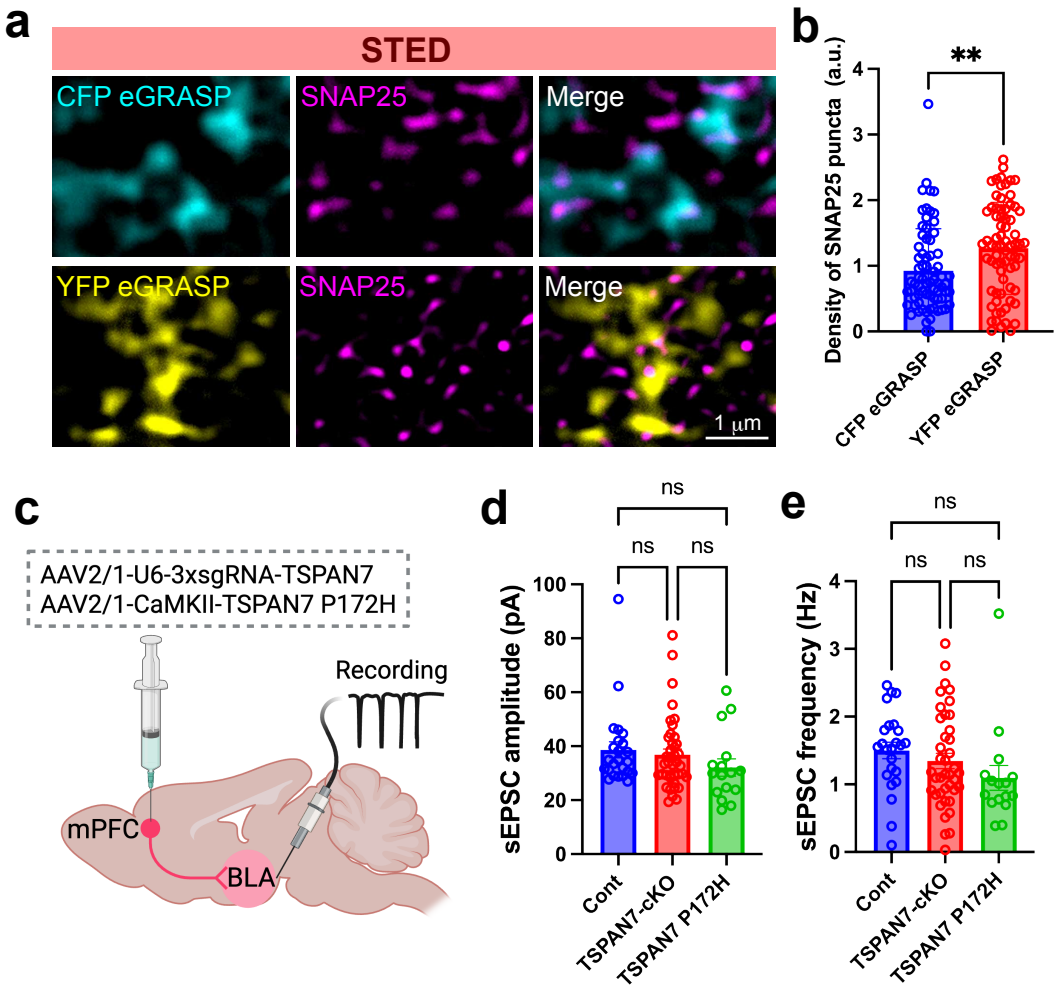

Extended Data Fig. 7. Presynaptic SNAP25 enrichment and basal excitatory transmission in TSPAN7-manipulated mPFC–BLA synapses. **a**, Representative STED images showing SNAP25 immunoreactivity at CFP eGRASP–labelled and YFP eGRASP–labelled mPFC→BLA synapses in the BLA, together with merged views. Scale bar, 1 μm. **b**, Quantification of SNAP25 signal intensity at CFP eGRASP–positive mPFC→BLA synapses in the BLA, showing SNAP25 enrichment at general synapses and its alteration by TSPAN7 mutations. **c**, Schematic of whole-cell recording configuration used to assess spontaneous excitatory postsynaptic currents (sEPSCs) in BLA pyramidal neurons following circuit-specific TSPAN7 deletion or TSPAN7 P172H expression in mPFC→BLA neurons. **d–e**, Quantification of sEPSC amplitude (**d**) and frequency (**e**) in BLA pyramidal neurons across genotypes, revealing altered basal synaptic transmission in TSPAN7-deficient circuits. In **d** and **e**, data are mean ± s.e.m.; Control = 24 cells, TSPAN7-cKO = 40 cells and TSPAN7 P172H = 16 cells from 3–4 mice; one-way ANOVA with Tukey's multiple comparisons test; ****P < 0.0005.

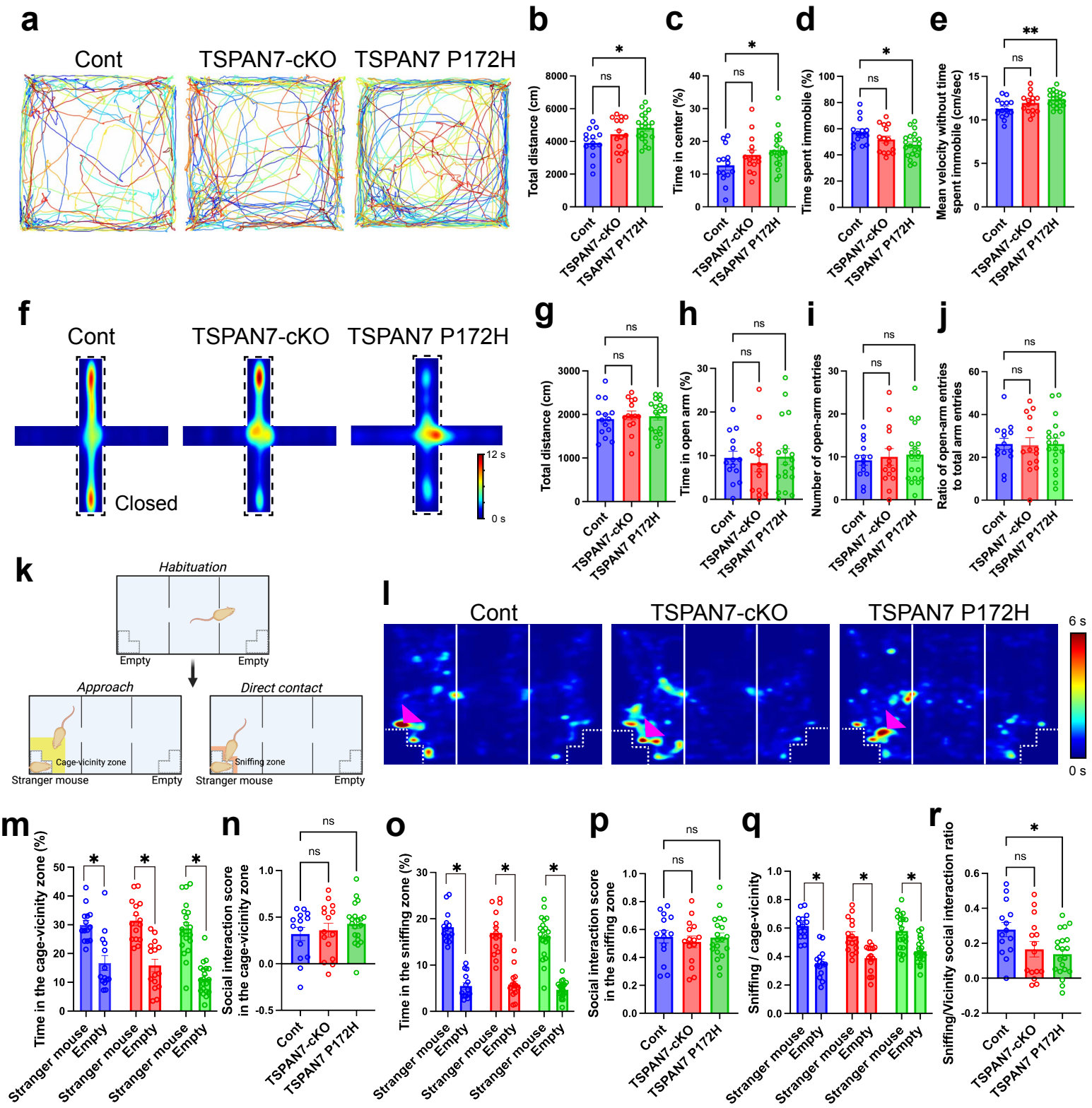

Extended Data Fig. 8. TSPAN7 loss and a disease-associated TSPAN7 variant cause mild hyperlocomotion and reduced close social investigation. **a**, Representative trajectory maps showing time spent in the open-field test. **b–e**, Quantification of total distance travelled (**b**), percentage of time spent in the centre zone (**c**), percentage of time spent immobile (**d**), and mean velocity excluding immobile periods (**e**) in the open-field test. **f**, Representative heatmaps showing time spent during the elevated plus maze (EPM) test. **g–j**, Quantification of total distance travelled (**g**), percentage of time spent in the open arms (**h**), number of open-arm entries (**i**), and proportion of open-arm entries (**j**) in the EPM. **k**, Schematic of the three-chamber social interaction test, indicating the cage-vicinity and sniffing zones. **l**, Representative heatmaps showing time spent during the three-chamber social interaction test. **m–r**, Quantification of percentage of time spent in the cage-vicinity zone (**m**), social-interaction score in the cage-vicinity zone (**n**), percentage of time spent in the sniffing zone (**o**), social-interaction score in the sniffing zone (**p**), ratio of interaction time in the sniffing zone to that in the cage-vicinity zone (**q**), and ratio of social-interaction scores in the sniffing zone to those in the cage-vicinity zone (**r**). In **b-e**, data are mean ± s.e.m.; control =14, TSPAN7-cKO = 15 and TSPAN7 P172H = 20 mice from 4 independent experiments; one-way ANOVA with Dunnett's multiple comparisons test; *P < 0.05, **P < 0.01. In **g-j**, data are mean ± s.e.m.; control =14, TSPAN7-cKO = 14 and TSPAN7 P172H = 19 mice from 4 independent experiments; one-way ANOVA with Dunnett's multiple comparisons test; ns= not significant. In **m, o, q**, data are mean ± s.e.m.; control =14, TSPAN7-cKO = 15 and TSPAN7 P172H = 20 mice from 4 independent experiments; Student's t-test; *P < 0.05. In **n, p, r**, data are mean ± s.e.m.; control =14, TSPAN7-cKO = 15 and TSPAN7 P172H = 20 mice from 4 independent experiments; one-way ANOVA with Dunnett's multiple comparisons test; ns= not significant, *P < 0.05.

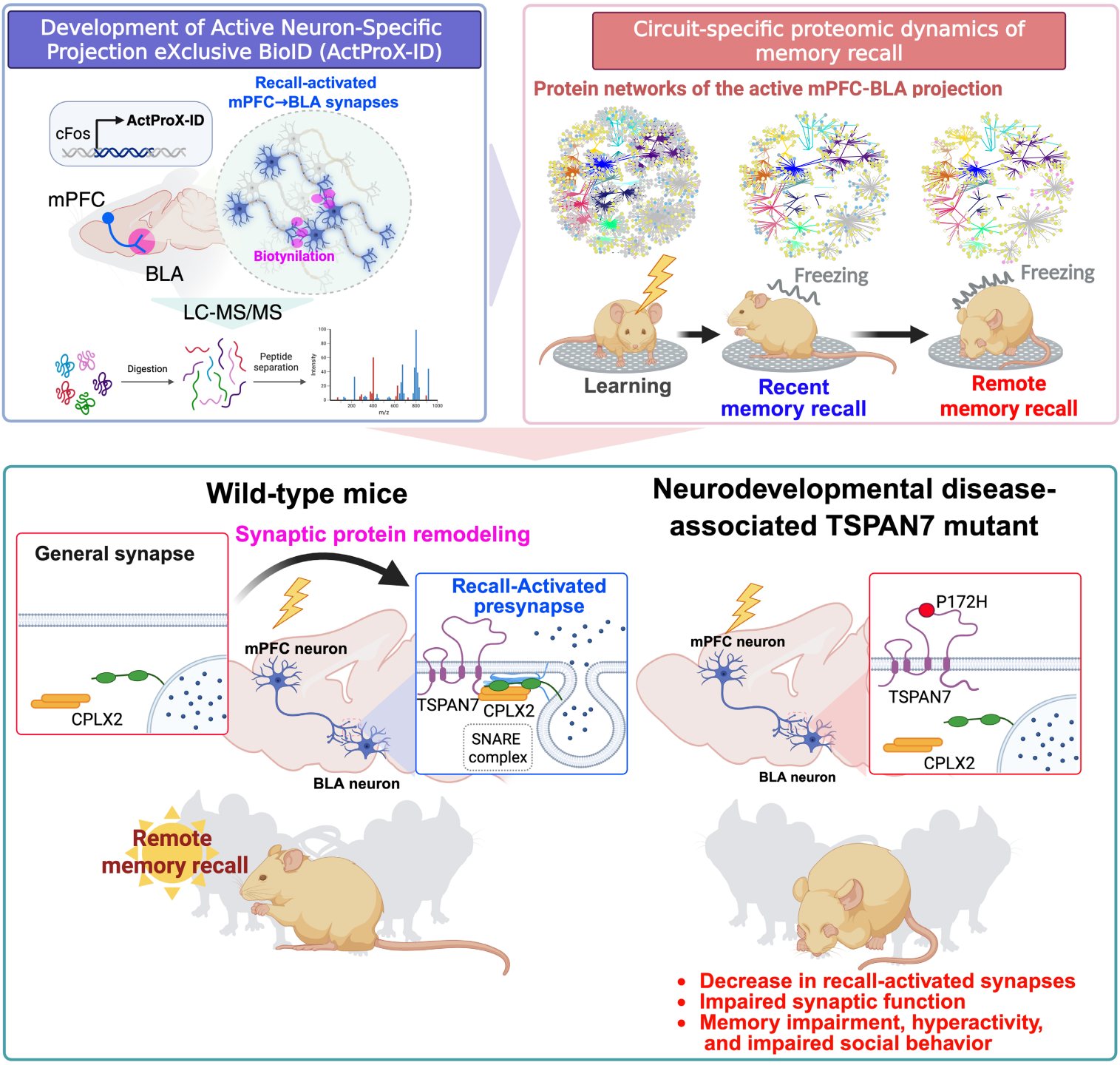

Extended Data Fig. 9. ActProX-ID identifies a recall-activated TSPAN7–CPLX2 presynaptic module that supports remote memory recall and socioemotional behaviour. We developed Active Neuron-specific Projection-eXclusive BioID (ActProX-ID), which drives expression of a presynaptic TurboID construct in activity-tagged mPFC neurons projecting to the BLA, enabling biotinylation of proteins at recall-activated mPFC→BLA synapses for LC–MS/MS analysis. ActProX-ID resolves circuit- and phase-specific presynaptic proteomic states, revealing distinct presynaptic modules engaged during recent versus remote fear memory recall. Among these, a TSPAN7–CPLX2 module is selectively recruited to active presynaptic sites in the mPFC→BLA pathway, where it promotes SNARE complex assembly, supports synaptic function and enables remote memory recall together with normal socioemotional behaviour. In contrast, the neurodevelopmental disease–associated TSPAN7 P172H variant reduces the number of active synapses, impairs presynaptic function and diminishes TSPAN7/CPLX2 recruitment, resulting in deficits in remote memory recall and social behaviour with increased anxiety-like traits.